Environmental Modelling & Software 94 (2017) 127–139

Contents lists available at ScienceDirect

Environmental Modelling & Software

journal homepage: www.elsevier.com/locate/envsoft

Application of the space-for-time substitution method in validating long-term biomass predictions of a forest landscape model

Jun Ma [a], Xiangming Xiao [a, b, *], Rencang Bu [c], Russell Doughty [b], Yuanman Hu [c], Bangqian Chen [a, d], Xiangping Li [a], Bin Zhao [a]

[a] *Ministry of Education Key Laboratory for Biodiversity Science and Ecological Engineering, Institute of Biodiversity Science, Fudan University, Shanghai, 200433, PR China*

[b] *Department of Microbiology and Plant Biology, Center for Spatial Analysis, University of Oklahoma, Norman, OK 73019, USA*

[c] *Institute of Applied Ecology, Chinese Academy of Sciences, Shenyang, 110016, PR China*

[d] *Danzhou Investigation & Experiment Station of Tropical Cops, Ministry of Agriculture, Rubber Research Institute, Chinese Academy of Tropical Agricultural Sciences (CATAS), Danzhou 571737, PR China*

A R T I C L E I N F O

Article history:
Received 29 April 2016
Received in revised form
6 April 2017
Accepted 14 April 2017

Keywords:
Forest landscape models
LANDIS-II model
Forest biomass
Forest age
Space-for-time
Northeastern China

A B S T R A C T

Validation of the long-term biomass predictions of forest landscape models (FLMs) has always been a challenging task. Using the space-for-time substitution method, forest biomass curves over stand age were generated from a forest survey dataset (FSD) in the Lesser Khingan Mountains area (*LKM*), Northeastern China and compared with long-term biomass predictions of LANDIS-II model. The results showed that mean forest age and mean biomass of the *LKM* in 2000 were 51.6 years and 84.2 Mg ha^{-1}, respectively. Significant linear correlations were found between FSD derived biomass and simulated biomass in the aggradation phase for the entire *LKM* and most subregions. However, a considerable difference in the mean maximum biomass (53.45 Mg ha^{-1}) existed between from FSD and simulation during the post-aggradation phase. The space-for-time substitution method has potential in validating time series biomass predictions of FLMs in aggradation phase when only limited forest inventory data is available.

© 2017 Elsevier Ltd. All rights reserved.

1. Introduction

Forests are a key component of terrestrial ecosystems and play an important role in the global carbon cycle (Birdsey et al., 2006; Dixon et al., 1994; Houghton and Hackler, 2000). Predictions of forest biomass and its spatial distribution are essential for evaluating how forests contribute to climate change mitigation (Keith et al., 2009; Saatchi et al., 2011). Forest landscape models (FLMs) are generally used to simulate forest biomass, species composition, and stand structure at large spatiotemporal extents (Gustafson et al., 2010; He et al., 1999; Scheller et al., 2007; Scheller and Mladenoff, 2004). The effects of forest management (Scheller et al., 2011a, 2011b), climate change (He et al., 2005; Ma et al., 2014b), and disturbances (He and Mladenoff, 1999) on forest succession dynamics, such as biomass accumulation and species distribution, can also be explored in FLMs. However, the credibility of predictions, especially forest biomass, directly determines the scope and applicability of FLMs in forest management (Gardner and Urban, 2003; Shifley et al., 2009; Tian et al., 2016; Wang et al., 2014b). Thus, it is important to evaluate FLMs predictions with observational data.

Traditionally, the evaluation of simulated results of most FLMs is conducted by comparing the predictions with results from empirical knowledge, other model outputs, and/or field observation data (Blanco et al., 2007; Busing et al., 2007; Ma et al., 2014a). For example, field collected data were used to validate the phenological predictions of the PHENIPS model in Bohemian forests (Berec et al., 2013). The productivity and cycling of carbon and nitrogen in aspen forests were simulated in five different models, and the results from multiple models were cross validated (Wang et al., 2014a). Monthly carbon flux data were used to calibrate and validate the results of the LANDIS-II model, which was used to simulate forest carbon sequestration under different fire regimes (Scheller et al., 2011b). A TROLL simulation of tropical rainforest spatial patterns was compared to field sampling data to validate predicted forest succession processes (Chave, 1999). However, most validations of FLMs

* Corresponding author.
E-mail address: xiangming.xiao@ou.edu (X. Xiao).

http://dx.doi.org/10.1016/j.envsoft.2017.04.004
1364-8152/© 2017 Elsevier Ltd. All rights reserved.

Model description

Model name LANDIS-II
Developers Eric Gustafson, USDA Forest Service; David Mladenoff, University of Wisconsin-Madison; Robert Scheller, Portland State University; Brain Stuturvant, USDA Forest Service; Jonathan Thompson, Harvard Forest
Contact Information Dr. Robert Scheller, Department of Environmental Sciences and Management, Portland State University. Email: rmschell@pdx.edu
Year First Available 2004
Hardware Required No special requirements
Software Required Windows, Mac OSX, or Linux
Availability Free (downloading site: http://www.landis-ii.org/install)
Program Language C#
Data Form of Repository Files and Spreadsheet

predictions were conducted at a specific site and time, which do not match the large spatiotemporal extents used in FLM simulations.

One of the ideal methods to improve the short-term predictions of FLMs is to conduct model calibration by comparing model predictions with time-series in-situ field data at appropriate spatiotemporal scales (Schmitz, 1997; Tsoar et al., 2007; Zaniewski et al., 2002). The model calibration has been proved to improve the credibility of predictions in ecological models based on a large amount of ecological data (Marcot et al., 2006; Wang et al., 2014b). Forest inventory data has been adopted by forest modeling studies to calibrate and validate predictions made by ecological models, which has enhanced the performance of the models (Peng et al., 2011). FLMs are parameterized using complex field-collected data at landscape scale, and the validation of FLM results, generally requires a multitude of long-term observation data. However, this kind of data is not available for most forest areas in the world. Chronological forest inventory data can be used effectively to improve the predictions of FLMs. For example, LANDIS Pro is a dynamic FLM that simulates processes like forest succession, seed dispersal, species establishment, and disturbances (Gustafson et al., 2000; He et al., 1999; Ma et al., 2014b). Biomass can also be simulated in this model by tracking tree species cohorts and their amounts of the landscape. A recent study proposed a framework for evaluating short-term predictions of the LANDIS Pro model based on a series of historical forest inventory data (Wang et al., 2014b).

Ground-based forest survey data, such as the U.S. Forest Inventory and Analysis (FIA) data, are increasingly abundant and easily obtained. However, similar data that are appropriate for comparison with the long-term predictions of FLMs are still scarce for forests in China. Theoretical and empirical knowledge are usually used to judge the long-term predictions and adjust the initial parameters of FLMs of forest regions in Northeastern China (He, 2008). Generally, different forest succession stages were regarded as representative moments of forest growing process, and measurements of their biomass have been used to predict the trajectories of forest carbon sequestration (Larsen et al., 2010; Ma et al., 2015; Wang et al., 2014b). However, great uncertainties exist in forest biomass accumulation over time when considering only specific states of succession. Also, climate change and disturbance influences forest biomass accumulation processes to a considerable extent (Chiang et al., 2008; Li et al., 2000; McMahon et al., 2010; Xu et al., 2012). Therefore, time series forest biomass survey data is essential for calibrating long-term FLM simulations, however, this data is difficult to acquire. Fortunately, based on the space-for-time substitution method, observed forest biomass at different stand ages can be used to compare with the long-term biomass predictions of FLMs.

Forest survey dataset (FSD) is generated based on different forest management units in China at regular intervals (every 10 years) and contain abundant information such as species composition, tree ages, and timber volume (Dong et al., 2008). From FSD, we can obtain information on the spatial distribution of vegetation communities, stand ages, and biomass. This dataset is commonly used to parameterize FLMs such as LANDIS Pro and LANDIS-II (Bu et al., 2008a; He et al., 2005). The space-for-time substitution method can be adopted to validate long-term forest biomass simulations by assuming that the biomass of old-growth forest is the future state of the younger forests. Therefore, this method might be useful for validating long-term biomass predictions of FLMs, especially when only limited forest inventory data is available.

In this study, the LANDIS-II model was used to illustrate how the space-for-time substitution method is applied to validate long-term biomass predictions based on FSD derived forest age and biomass data. FSD of 2000 was used to calculate forest biomass dynamics with different stand ages in different regions in the Lesser Khingan Mountains area (*LKM*) of Northeastern China, and the forest biomass-age curves were compared with simulated biomass of LANDIS-II model for the entire *LKM* and its subregions. The objectives of this study were to (1) generate forest biomass-age curves based on the FSD of the *LKM* in the year 2000; (2) simulate biomass dynamics from 2000 to 2300 using LANDIS-II model; and (3) explore the performance of the space-for-time substitution method in the validation of biomass predictions by the LANDIS-II model.

2. Materials and methods

2.1. Study area

The study area, extends across 47.05°–49.32° N, 127.02°–130.79° E, which covers the entire *LKM* (Fig. 1). The forest coverage ratio of the study area is about 73% and the elevation ranges between 400 m and 600 m above sea level. The topography changes from being mountainous in the northern part to having hills and low lying mountains in the southern portion of the study area. Dark brown soil is the major soil type, which is distributed throughout the region (Zhang et al., 2013). The *LKM* is dominated by temperate continental monsoon climate that is characterized by long cold winters (mean January temperature, −25 °C) and short warm summers (mean July temperature, 21 °C). The growing season generally lasts from late May to early October, and the precipitation occurs mostly in the summer with an average annual rainfall range between 550 and 670 mm. The entire *LKM* forest landscape includes twenty-one subregions (forest bureaus): *Zhanhe* (*ZH*), *Hongxing1* (*HX1*), *Wuyiling* (*WYL*), *Tangwanghe* (*TWH*), *Shanggangling1* (*SGL1*), *Xinqing* (*XQ*), *Youhao* (*YH*), *Wuying* (*WY*), *Hongxing2* (*HX2*), *Tongbei* (*TB*), *Shanggangling2* (*SGL2*), *Hebei* (*HB*), *Lilin* (*LL*), *Shanggangling3* (*SGL3*), *Fenglin* (*FL*), *Suiling* (*SL*), *Meixi* (*MX*), *Cuiluan* (*CL*), *Wumahe* (*WMH*), *Jinshantun* (*JST*), and *Tieli* (*TL*).

The *LKM* is a transitional zone between cold and moderate temperate climate zones, and therefore it contains coniferous forests in the north, mixed coniferous-broadleaf forests in the central area, and broadleaf forests in the south. The dominant tree species include Korean pine (*Pinus. koraiensis*), Spruce (*Picea koraiensis and P. jezoensis*), Khingan fir (*Abies nephrolepis*), Larch (*Larix gmelinii*), Mongolian Scotch pine (*Pinus sylvestris Linn.*), Manchurian walnut (*Juglans mandshurica*), Manchuria ash (*Fraxinus mandshurica*),

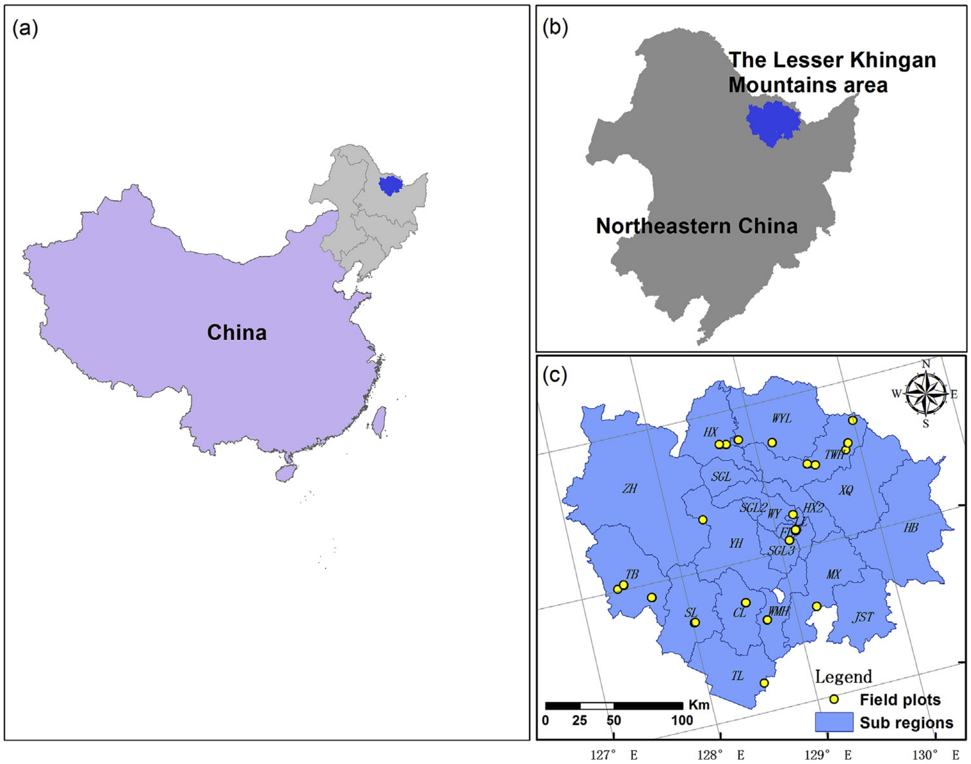

Fig. 1. Study area and locations of forest sampling plots in the Lesser Khingan Mountains area of Northeastern China. (a) Northeastern China in China, (b) The Lesser Khingan Mountains area in Northeastern China, and (c) The forest bureaus boundaries and forest sampling plots.

Amur cork (*Phellodendron amurense*), Mongolia oak (*Quercus mongolica*), Black elm (*Ulmus propinqua*), Mono maple (*Acer mono Maxim*), Ribbed birch (*Betula costata*), Black birch (*Betula davurica*), Amur linden (*Tilla amurensis*), White birch (*Betula platyphylla*), Aspen (*Populus davidiana*).

2.2. Forest survey dataset (FSD)

Forest survey dataset (FSD) of the *LKM* are usually generated every 10 years, and the FSD in 2000 was available for this study. This dataset was produced by the Forestry Planning and Design Bureau of Heilongjiang Province in 2003. The *LKM* contains 21 forestry bureaus, and each forestry bureau is divided into several forest management units (about 10 ha per unit). For each individual management unit, species composition, tree age and density, and timber volume were surveyed. The collected data was input into a vector format dataset. For this study, we converted the vector dataset into several 90 m-resolution raster layers including the map of species composition, forest stand age (Fig. 2), and timber volume. In order to match with the ecoregions map (which was converted from 90-m resolution DEM data) and to fit the operating ability of the computer, all the raster layers were set at 90-m resolution, and this resolution was higher than that of most previous LANDIS-II simulation studies.

The value of a given pixel in the forest age map was the mean age of all tree species in that pixel. The forest species composition map was used in the parameterization of LANDIS-II model. For the entire *LKM* and each subregion, we calculated the mean, median, and standard deviation of stand age (Table 1). In order to match the output of LANDIS-II model, forest ages were grouped into bins at 10-year intervals. Based on the 10-year time step, the mean stand ages for most subregions are equal to their respective median values (Table 1). Therefore, it is applicable to use the mean forest

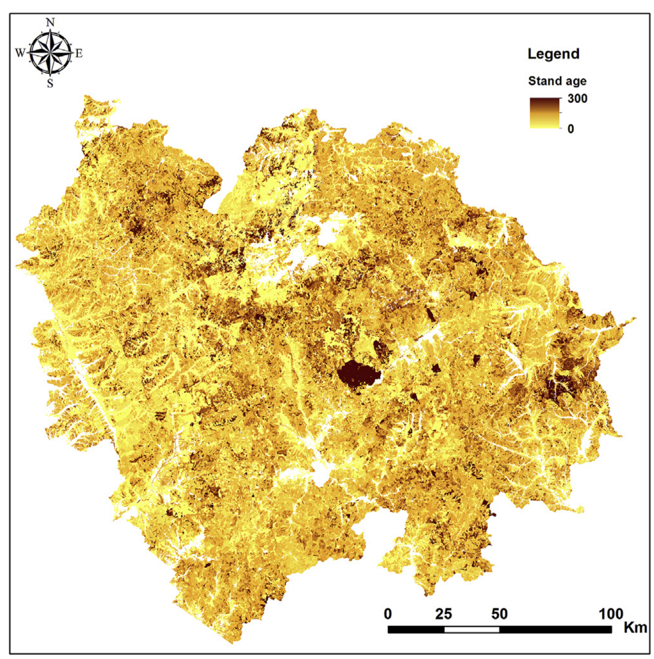

Fig. 2. Distribution of forest stand ages map in the Lesser Khingan Mountains area of Northeastern China.

age as an approximation of forest age in each subregion.

Considering the forests in the *LKM* experienced severe disturbance in history, we divided the forest biomass accumulation curve in this study into three phases based on a previous study that focused on forest biomass dynamics after disturbances (Bormann

Table 1
Forest area, stand age, and biomass (calculated from timber volume information in forest survey dataset) of different subregions (forestry bureau) and the entire Lesser Khingan Mountains area for the year of 2000. Mean, median, and STD represent the mean, median, and stand deviation values of forest stand age. Min, Max, Mean, Median, and STD represent the minimum, maximum, mean, median, and stand deviation values of initial biomass in 2000.

Regions	Area(Km^2)	Stand Age			Forest biomass (Mg ha^{-1})				
		Mean	Median	STD	Min	Max	Mean	Median	STD
Zhanhe (ZH)	7599.1	50.2	50	17.1	26.27	199.61	74.39	78.93	24.95
Hongxing1 (HX1)	1858.5	43.0	40	23.4	29.02	179.17	66.72	50.64	34.62
Wuyiling (WYL)	3183.1	53.7	50	12.4	28.99	175.56	78.35	79.03	19.03
Tangwanghe (TWH)	2254.0	56.8	60	23.2	26.37	201.75	82.15	77.60	32.99
Shanggangling1 (SGL1)	665.4	43.1	40	23.3	34.64	183.97	68.42	69.54	32.67
Xinqing (XQ)	2926.7	48.0	50	23.6	26.81	198.72	71.54	70.31	29.36
Youhao (YH)	2830.6	52.0	50	23.7	28.85	198.98	76.53	71.38	34.72
Wuying (WY)	1214.4	52.7	50	31.6	27.80	210.09	74.93	69.38	38.66
Hongxing2 (HX2)	881.8	46.5	40	21.4	26.60	193.52	66.53	61.53	30.18
Tongbei (TB)	2693.7	44.4	50	16.0	26.27	171.54	68.69	74.28	21.63
Shanggangling2 (SGL2)	157.8	55.6	50	17.0	40.51	159.77	85.47	65.79	40.98
Hebei (HB)	3903.8	56.7	50	29.1	26.99	212.83	86.04	79.87	40.74
Lilin (LL)	81.1	68.0	50	34.8	40.10	189.52	100.99	73.09	53.53
Shanggangling3 (SGL3)	634.6	50.4	50	19.4	30.79	213.40	71.42	70.88	23.68
Fenglin (FL)	180.0	161.6	170	41.3	55.33	197.52	174.30	181.62	29.51
Suiling (SL)	2171.2	47.3	50	19.9	26.22	202.38	73.15	73.11	29.02
Meixi (MX)	2264.1	51.6	50	18.9	26.55	217.65	77.67	77.74	28.50
Cuiluan (CL)	1558.4	44.9	40	18.4	26.85	190.66	65.09	64.51	22.26
Wumahe (WMH)	1239.5	42.7	40	12.8	26.33	184.89	66.21	67.57	20.36
Jinshantun (JST)	1852.2	54.2	50	24.4	29.46	205.87	79.24	78.92	29.98
Tieli (TL)	2042.0	50.9	50	20.7	26.91	208.06	77.81	76.77	30.50
Entire landscape (LKM)	42191.9	51.6	50	24.6	26.22	217.65	84.16	75.78	31.54

and Likens, 1979): reorganization, aggradation, and post-aggradation. During the reorganization phase, which is a period following disturbance, the rate of biomass accumulation is low. Then, we define the beginning of the aggradation phase as the time when biomass increases 30% or more between two time steps. The post-aggradation phase begins when forest biomass increases less than 5% between two time steps, and forest age of the beginning of this phase is regarded as the stable age. The post-aggradation phase may include a transition period in which forest biomass declines after reaching its peak (Perry et al., 2008). In this study, we mainly compared simulated biomass and FSD derived biomass of the aggradation phases of the *LKM* and each subregion, the aggradation phase was marked in Figs. 4 and 5.

2.3. Model parameterization

LANDIS-II is a cellular automaton FLM that simulates forest succession, seed dispersal, species establishment, and the impact of disturbances on the forest (He and Mladenoff, 1999; Mladenoff, 2004; Mladenoff and He, 1999b; Scheller et al., 2007). LANDIS-II is derived from an earlier version of LANDIS, which simulates forest landscape processes using a grid of cells. The cell size ranges from 10 m to 500 m, and large spatial ($<10^8$ ha) and temporal ($<10^3$ years) extents can be simulated. In each cell, all trees were grouped into different species cohorts, and they were tracked through the whole simulation period in LANDIS-II. Based on species stand age and species composition, forest biomass of each cell and each species was calculated (Scheller and Mladenoff, 2004). In order to reflect the heterogeneity of the simulated landscape and the differences in growing conditions (temperature, light, and precipitation) among forest stands, three raster layers (altitude, aspect, and watershed boundaries) were combined to delineate ecoregions. Using this approach, the entire study area was divided into 166 ecoregions (Fig. S1a). The ecoregions map is an important input parameter for the LANDIS-II model. Each ecoregion varies from the other and represents a unique habitat for forest growing. For each ecoregion, the establishment probability of each tree species varies from the other. For each species, its establishment probabilities also vary among different ecoregions. The initial communities map is another important input parameter (Fig. S1b), and it was generated mainly by adjusting the species composition map, which was converted from FSD. Details about the simulation mechanisms of ecological and spatial process in LANDIS-II model can be found and consulted in previous studies (Gustafson et al., 2010; Scheller et al., 2007, 2008; Scheller and Mladenoff, 2004).

Sixteen tree species (Fig. S2), including five conifers and eleven broadleaf species, were simulated in this study. Forest succession in the LANDIS-II model is driven by species' biological attributes (Table 2), which were collected from previous studies and indigenous empirical knowledge (Bu et al., 2008a; Ma et al., 2014b). The LANDIS-II model was run for 300 years (from 2000 to 2300) at a 10-year time step. Forests in Northeastern China have experienced severe deforestation in the past several decades, but since 2000 they have been the key focus of the Natural Forest Resource Conservation Project (Wei et al., 2014). Harvest of forests in *LKM* is now entirely forbidden. Therefore, no timber harvesting was simulated in this study. Although rigorous fire suppression is practiced in the *LKM*, lightning fires can occur under some weather conditions (when the fuel load is high and dry). The occasionality of the occurrence of fire disturbance in this area at spatial and temporal scales is quite high, and the fire distribution can be regarded as random. Therefore, a random fire regime based on fuel types was simulated in the "Dynamic Fire System" extension, based on fuel types, which were calculated from Canadian Fire Behavior Prediction System (Forestry Canada Fire Danger Group, 1992) using parameters that were converted from species-cohort information in the LANDIS-II model.

The "Biomass Succession" extension in LANDIS-II model was used to simulate forest biomass in this study. In the simulation, species establishment probability (SEP) and maximum aboveground net primary productivity ($ANPP_{max}$) are two important parameters. SEP and $ANPP_{max}$ can directly determine the results of biomass and indirectly reflect the impact of climate on simulated biomass. A site-level ecosystem model, PnET-II, was used to simulate SEP and $ANPP_{max}$ in this study. The PnET-II model was developed to simulate vegetation growth processes, biomass

Table 2
Biological (life history) attributes of main species in the Lesser Khingan Mountains area. LONG: Longevity; MTR: Mature age; ST: Shade tolerance; FT: Fire tolerance; ESD: Effective distance of seed disperse; MSD: Maximum distance of seed disperse; VP: Vegetative production probability; SA_{min}: Minimum age of sprout age; SA_{max}: Maximum age of sprout age; PFRR: Post-fire regeneration regime. Shade tolerance is an ordinal scale whereby 1 is the least shade tolerant, 5 is the most tolerant. Fire tolerance is an ordinal scale whereby 1 is the least fire tolerant, 5 is the most tolerant.

Species	LONG (a)	MTR (a)	ST	FT	ESD (m)	MSD (m)	VP	SA_{min} (a)	SA_{max} (a)	PFRR
Korean pine (*Pinus. koraiensis*)	450	80	4	3	200	600	0	0	0	None
Spruce (*Picea koraiensis and P. jezoensis*)	300	30	4	3	80	200	0	0	0	None
Khingan fir (*Abies nephrolepis*)	200	30	4	3	80	200	0	0	0	None
Larch (*Larix gmelinii*)	300	20	3	4	80	200	0	0	0	None
Mongolian scotch pine (*Pinus sylvestris Linn.*)	250	20	1	1	100	200	0	0	0	Resprout
Manchurian walnut (*Juglans mandshurica*)	250	15	1	2	50	100	0.9	60	70	Resprout
Manchuria ash (*Fraxinus mandshurica*)	250	40	3	5	400	1000	0.9	50	110	None
Amur cork (*Phellodendron amurense*)	250	15	3	4	60	300	0.8	60	90	None
Mongolia oak (*Quercus mongolica*)	320	20	3	5	50	200	1	50	100	Resprout
Black elm (*Ulmus propinqua*)	250	10	3	3	200	1000	0.5	60	100	None
Mono maple (*Acer mono Maxim*)	200	10	3	3	500	1000	0.5	50	60	None
Ribbed birch (*Betula costata*)	250	15	3	3	500	4000	0.9	40	90	Serotiny
Black birch (*Betula davurica*)	150	15	3	5	500	4000	0.9	30	50	None
Amur linden (*Tilla amurensis*)	300	15	3	2	80	250	0.8	30	80	None
White birch (*Betula platyphylla*)	150	15	1	2	500	4000	0.8	50	60	None
Aspen (*Populus davidiana*)	150	10	1	1	600	5000	0.9	10	60	None

accumulation, and forest productivity (Gustafson et al., 2010; Xu et al., 2007) based on climatic (temperature, precipitation, and irradiation), environmental (soil nutrition and water availability), and physiological (Table S1) parameters.

In this study, we ran PnET-II to get SEP and $ANPP_{max}$ for each ecoregion. In order to make the model reach a steady state, climate data from 1960 to 2000, which was compiled from 133 weather stations in northeastern China, was interpolated into the entire Northeastern China and then used in the PnET-II model. Further, in order to simulate the current climate of the forest landscape, the mean temperature and precipitation of the past 30 years (1970–2000, Fig. S2) was used as the input climate data of 2000 in the PnET-II model. The LANDIS-II model considered spatial heterogeneity in the ecoregions map parameter. The variation of climate is reflected in the various forest ecoregions, and the impacts of spatial variation on biomass were already reflected in the modeling results. Therefore, it has little impact on the application of the space-for-time substitution approach. Moreover, considering the great uncertainty of future climate, we parameterized the model of the initial year (2000) and assumed the climate change trend will remain the same level in period of 1970–2000. Climate change and variability are indirectly incorporated in LANDIS-II model. Climate data is used in the parametrization of PnET-II model to simulate ANPP and SEP, which are two important input parameters in biomass simulation in LANDIS-II model (Fig. 3). Therefore, climate change can be incorporated the in LANDIS-II simulations by setting SEPs of tree species at different future time, while spatial variation of climate can also be reflected in the parameter of different environmental factors in different ecoregions. In total, we simulated SEP and $ANPP_{max}$ of the sixteen tree species for 166 ecoregions.

The whole modeling process of LANIDS-II and PnET-II, as well as the derivations of the main parameters, are shown in a flow chat (Fig. 3). The LANDIS-II and PnET-II model ran five times, and the mean values were presented as the final results. Considering the difference among each running was quite small, we did not add error bars in the demonstration of the simulated biomass results.

2.4. Calculation of forest biomass

Using the maps of species composition and timber volume that were generated from FSD, we calculated forest biomass in 2000 using the relationship between biomass and timber volume (Fang et al., 1996, 1998). Based on the forest biomass and forest stand age maps, we set a series random points (20000 points) and extracted the pixel values of biomass and forest ages at relevant positions (Fig. S1c). Therefore, a dynamic curve of forest biomass of the *LKM* that varied with forest ages was generated. Similarly, dynamic curves of biomass in each subregion were also generated by using the same method. The minimum, maximum, mean, median, and standard deviation values of biomass for the *LKM* and each subregion are listed in Table 1. The simulated total biomass of the *LKM* and each subregion were also calculated. The observed mean forest ages of the *LKM* and each subregion in 2000 were regarded as the forest ages of these areas. Simulated forest biomass accumulation dynamics can also be divided into the three successional phases (reorganization, aggradation, and post-aggradation). Thus, simulated biomass from the LANDIS-II model and FSD derived biomass can be compared during the aggradation phase. All the data processing and mapping were conducted using “*raster*” package in *R* software and ArcGIS 10.3.

In this study, we also used some biomass data from forest field sampling plots to validate the simulated biomass at the site scale. The field investigation was conducted in 2011 and 2012, and a total of 64 forest plots with the size of 20 m × 50 m were surveyed. For each plot, the central point (latitude and longitude) was recorded. The species names, diameter at breast height (DBH), and height of individual trees in the overstory layer (DBH >5 cm or height >2 m) were also recorded. DBH-based allometric equations from previous studies (Chen and Zhu, 1989; Wang, 2006) were adopted to calculate tree biomass of each plot. The observed forest plot biomass was used to validate the simulated biomass in 2010 from the LANDIS-II model at the site scale.

2.5. Validation of biomass predictions

At the site scale, forest plot biomass measured in 2011 and 2012 was used to evaluate the LANDIS-II simulated biomass in 2010 for each location. We set a hypothesis that samples the field observed biomass and LANDIS-II simulated biomass in 2010 belong to a same population. In order to test this hypothesis, a *t*-test was conducted between field observed biomass and simulated biomass in 2010. Moreover, linear regression analysis was also used to detect the relationship between the two biomass datasets.

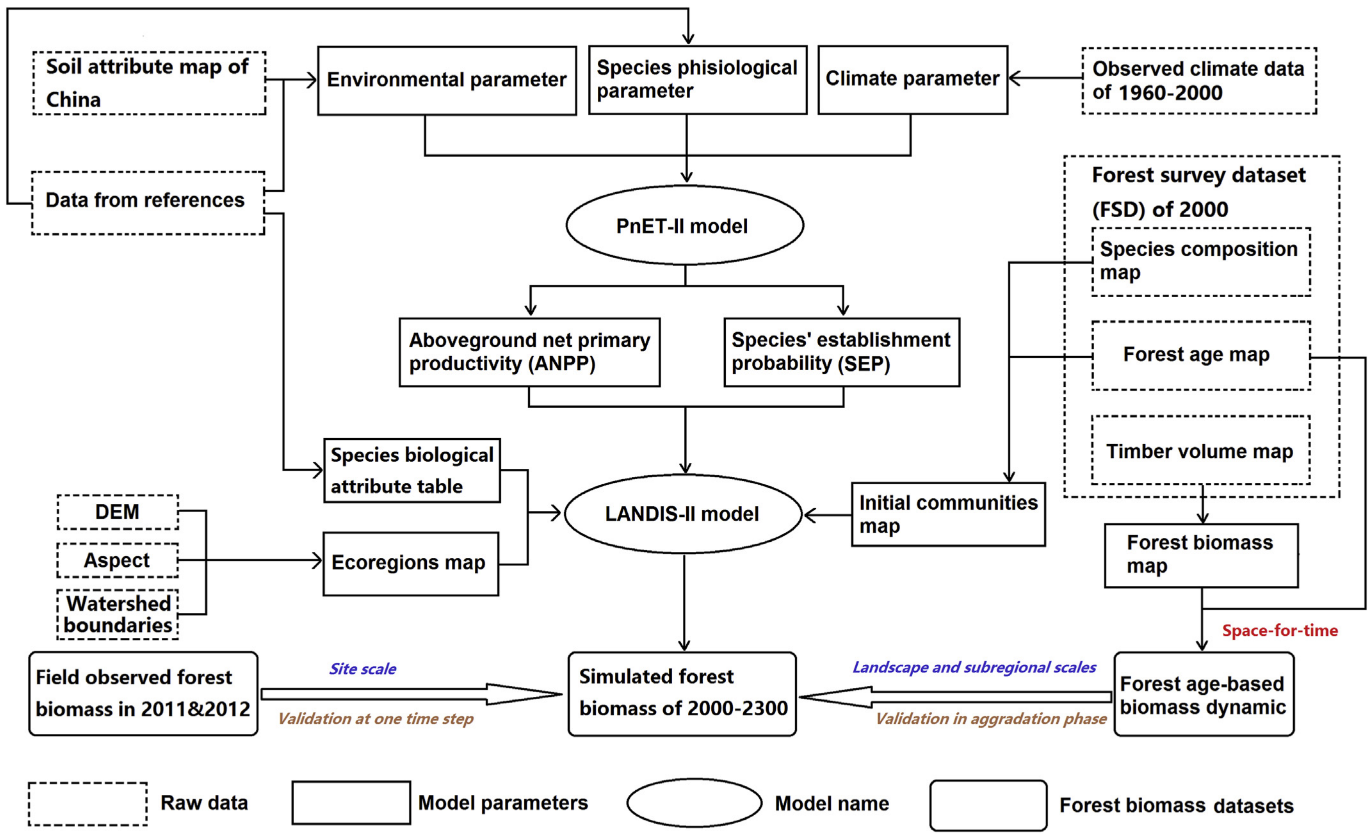

Fig. 3. Flow chat of the whole simulation and validation processes, including the main parameters of the LANDIS-II and PnET-II models and their derivations.

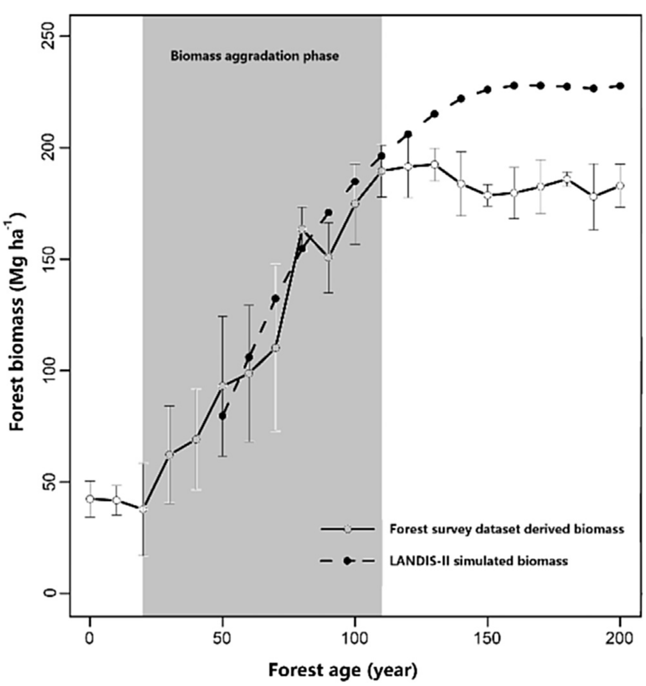

Fig. 4. Comparison between LANDIS-II simulated biomass and FSD derived biomass using the space-for-time method at the landscape scale. Grey background represents the aggradation phase of biomass accumulation.

At the landscape scale, we compared simulated biomass in the LANDIS-II model and FSD derived biomass in the aggradation phase of the *LKM* and each subregion (Figs. 4 and 5). T-test and linear regression analysis were also conducted between the two biomass datasets, and the correlation (R^2) and slope (k) of the regression line were used to estimate the relationship between simulated biomass and FSD derived biomass. Higher R^2 values means stronger linear relationship, while values of k closer to 1 illustrate better accuracy of biomass predictions. Moreover, root mean square error (*RMSE*) and the Nash-Sutcliffe index of mean error (*ME*) were used to estimate the quality of the comparison results. Lower values of *RMSE* reflect lower errors between actual biomass and simulated biomass, while values of *ME* closer to 1 indicate better accuracy of biomass predictions (Miehle et al., 2006). *RMSE* and *ME* were calculated using the following equations:

$$RMSE = \sqrt{\frac{\sum_{i=1}^{n}(BF_i - BS_i)^2}{\mathrm{n}}} \tag{1}$$

$$ME = 1 - \frac{\sum_{i=1}^{n}(BF_i - BS_i)^2}{\sum_{i=1}^{n}(BS_i - BS_{\mathrm{mean}})^2} \tag{2}$$

where n is sample size and i is the sequence number of sample; BF_i and BS_i represent the biomass of number i from the forest survey datasets and the simulated result in LANDIS-II model, respectively; BS_{mean} is the mean value of simulated biomass that was used in the comparison. All of the statistical analyses, including the t-test, correlation analysis, and the calculation of *RMSE* and *ME* were conducted using *R* software (R Development Core Team, 2011) with $P < 0.05$ used as a threshold of significance. A diagram of the comparisons between the two biomass datasets at site and landscape, subregional, and site scales was shown in Fig. 3.

In this study, we also compared the FSD derived biomass and

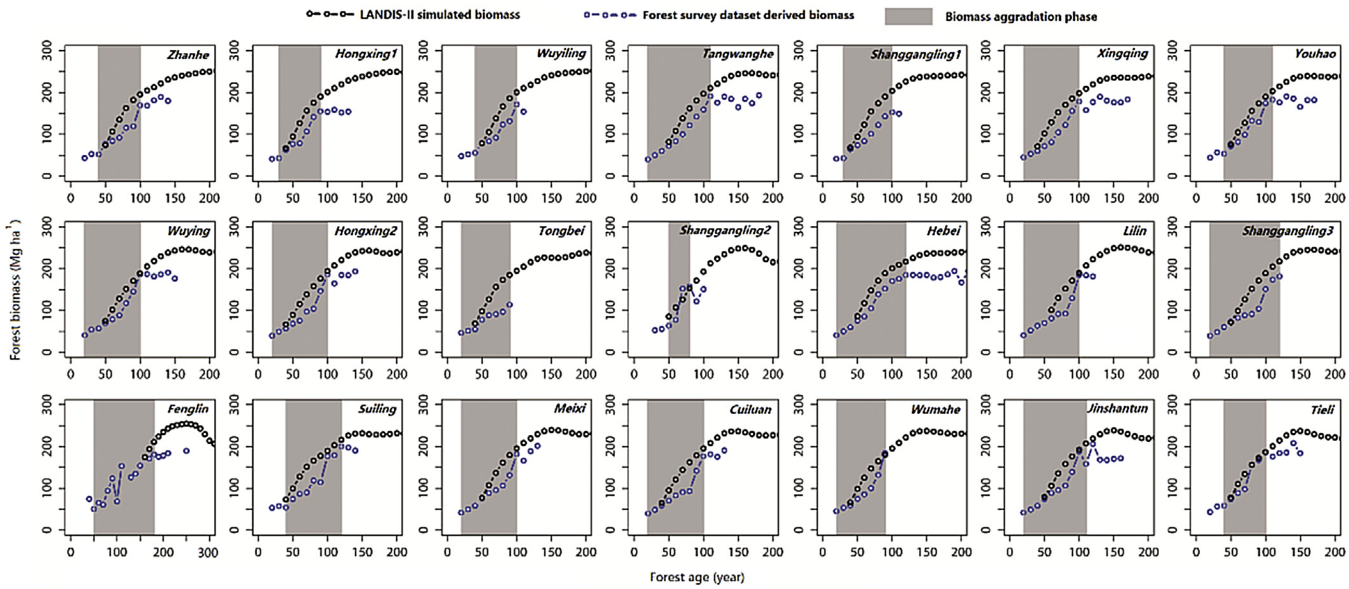

Fig. 5. Comparison between LANDIS-II simulated biomass and FSD derived biomass using the space-for-time method at the subregional scale. Grey background represents the aggradation phase of biomass accumulation.

simulated biomass in the post-aggradation phase. Mean biomass was at its maximum in this period. The mean value of the biomass in post-aggradation period was regarded as the mean maximum biomass (*MMB*). The *MMB* was calculated for the *LKM* and each subregion in both FSD derived biomass and LANDIS-II simulated biomass. The differences in *MMB* between simulated biomass and FSD derived biomass were also calculated. We checked the assumption of normality and homogeneity of variance for all variables in the statistical analysis of our study, and variables were natural logarithmically transformed when necessary.

3. Results

3.1. Forest ages and forest biomass from FSD

The mean forest age of the *LKM* in 2000 was about 51.6 years, and it ranged from 42.7 years in *WMH* to 161.6 years in *FL*. The median forest age of each subregions was between 40 and 50 years, while the standard deviations were generally less than 20 years (Table 1). Forest stand age was found to be highly variable across the *LKM*, and was illustrated in Fig. 2. The forest stand age is obviously higher in the reserve area (*FL*) and the eastern part of the *LKM*, while younger stands were almost often located in other regions.

The mean biomass for the *LKM* in 2000, derived FSD was 84.16 Mg ha^{-1}, and it ranged from 65.09 Mg ha^{-1} in *CL* to 174.30 Mg ha^{-1} in *FL*. The minimum, maximum, and median values of FSD derived biomass ranged from 26.22 Mg ha^{-1} in *CL* to 55.33 Mg ha^{-1} in *FL*, from 159.77 Mg ha^{-1} in *SGL2* to 217.65 Mg ha^{-1} in *MX*, and from 50.64 Mg ha^{-1} in *HX1* to 181.62 Mg ha^{-1} in *FL*, respectively (Table 1). Also, most of the standard deviations of forest biomass at subregional scale were less than 40 Mg ha^{-1}. Mean biomass calculated from FSD was highest in old growth forests, most notably the *FL* subregion (Fig. 6b). However, there was not much difference in FSD derived biomass of other subregions.

3.2. Spatial and temporal patterns of simulated forest biomass

Simulated total forest biomass of the *LKM* firstly increased from 79.6 Mg ha^{-1} in 2000 to 232.81 Mg ha^{-1} in 2100, then remained steady at about 237.97 Mg ha^{-1} in the period of 2100–2180. Biomass then dropped to 157.63 Mg ha^{-1} by 2230, but recovered to 230.05 Mg ha^{-1} by the end of the simulation (Table 1). As for spatial distribution, the total forest biomass in 2000 was relatively low in each subregion except *FL*. Biomass accumulation steadily increased for these other subregions until 2100, when biomass became comparable between *FL* and all of the subregions (Fig. 7). However, large spatial differences of total forest biomass can later be identified in 2200 when the forest biomass in southwestern part of the *LKM* became low. At the end of simulation, spatial differences of total forest biomass increased and declines of forest biomass can be identified in the eastern and northwestern parts of the *LKM*. However, biomass in the southwestern part of the *LKM* increased to high levels (Fig. 7).

3.3. Validation of simulated biomass using observed and FSD derived biomass

At the site scales, a significant (P < 0.05, R^2 = 0.468) linear correlation existed between field inventory biomass and simulated biomass in 2010 of the sampling sites (Fig. 8), while *t*-test result showed no significant (P = 0.078 > 0.05) difference between observed biomass and predicted biomass. However, most of the observed biomass was higher than that predicted by LANDIS-II model.

At the landscape and subregional scales, the difference between FSD derived biomass and simulated biomass in 2000 had high spatial heterogeneity (Fig. 6c). The difference between simulated biomass and FSD derived biomass for most subregions of the *LKM* ranged between −20 Mg ha^{-1} and 20 Mg ha^{-1}. The differences were greatest in the subregions that have high LANDIS-II simulated biomass.

High consistency and significant (P < 0.05) linear correlations were found between FSD biomass and simulated biomass in the aggradation phase for the entire *LKM* (Fig. 4), as well as for all subregions except *FL* (Fig. 5). The highest R^2 values existed in *HB*, while the value of k closest to 1 existed in *XQ* (Table 3). Moreover, *t*-test results also showed no significant (P > 0.05) differences

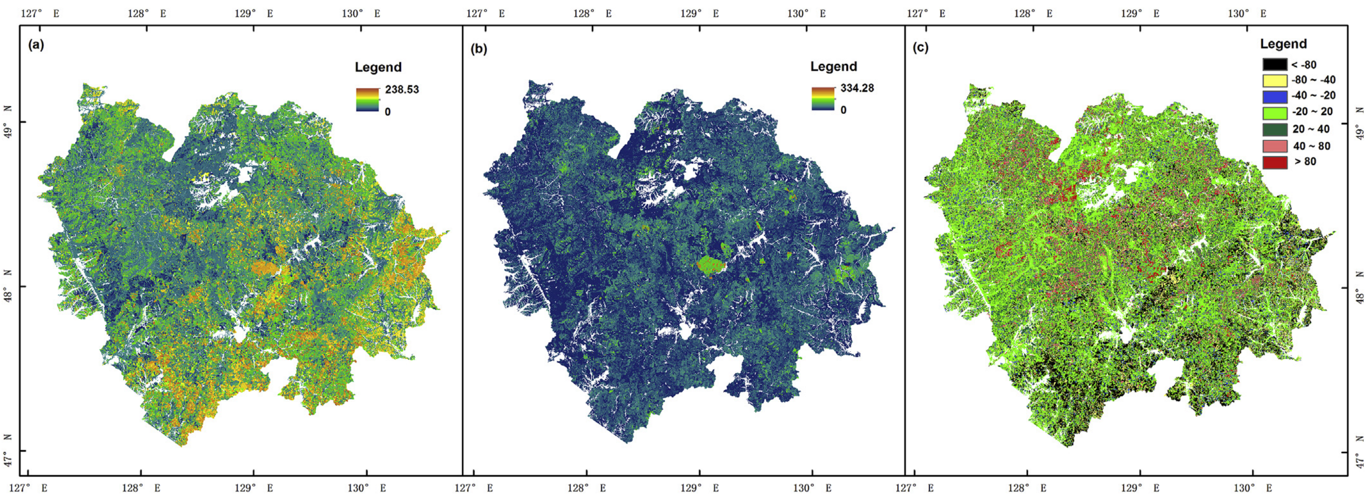

Fig. 6. Spatial distributions of simulated biomass from LANDIS-II, FSD derived biomass in 2000, and their difference. (a) LANDIS-II simulated biomass in 2000, (b) FSD derived biomass in 2000, and (c) The difference between FSD derived biomass and simulated biomass.

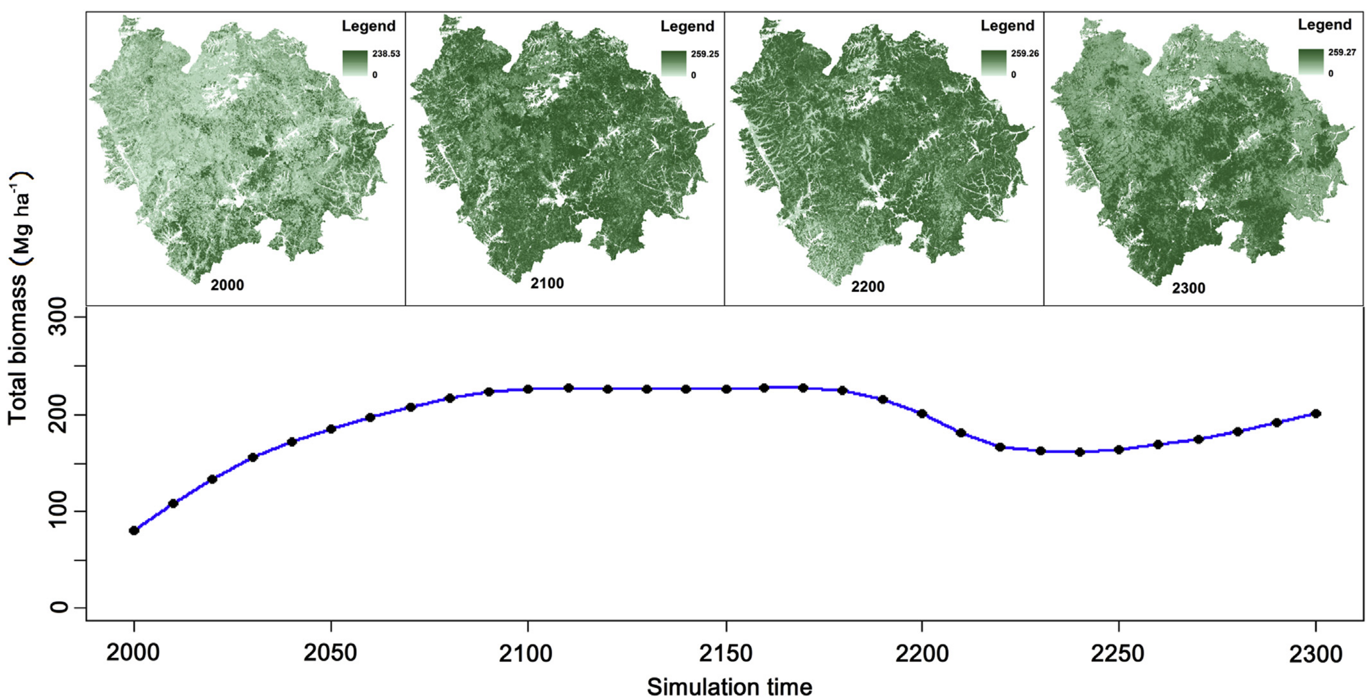

Fig. 7. Dynamics of simulated forest biomass from the LANDIS-II model in the Lesser Khingan Mountains area from 2000 to 2300. The four maps show the distribution of forest biomass every 100-year, and the curve shows the dynamic of forest biomass every 10-year of the entire landscape.

between these two biomass datasets for those regions (Table 3). Comparison results of the two biomass datasets in the aggradation phase showed that the values of *RMSE* ranged from 17.56 Mg ha^{-1} in the entire *LKM* to 53.27 Mg ha^{-1} in *TB*. The entire *LKM* also had the value of *ME* closest to 1 (Table 3).

3.4. Comparisons of mean maximum biomass in post-aggradation phase

In post-aggradation phase, the *MMB* derived from FSD varied between each region, and it ranged from 114.04 Mg ha^{-1} in *TB* with a 90-year age to 229.52 Mg ha^{-1} in *FL* with a 110-year age. Also, the *MMB* derived from simulated biomass ranged from 222.68 Mg ha^{-1} in *JST* with a 100-year age to 252.78 Mg ha^{-1} in *FL* with a 110-year age (Table 4). The differences in *MMB* between the two biomass datasets also varied among subregions, which ranged from 23.26 Mg ha^{-1} in *FL* to 123.49 Mg ha^{-1} in *TB*. However, the differences in *MMB* of the two biomass datasets was 53.45 Mg ha^{-1} at the landscape scale.

4. Discussion

4.1. Spatial and temporal dynamics of forest biomass

Data from the forest survey dataset was used to calculate forest biomass using a method established in a previous study (Fang et al.,

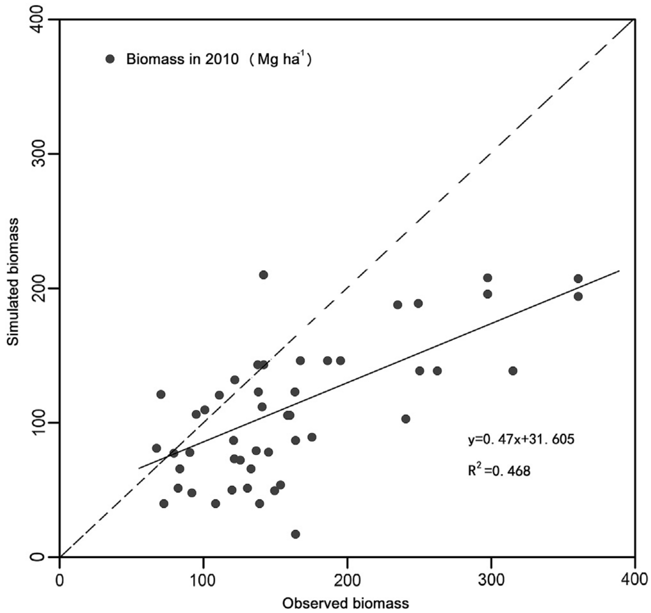

Fig. 8. The relationship between observed forest biomass and simulated forest biomass in 2010. Linear regression is used to fit the relationship, and asterisks after the R square values indicate significant correlations ($P < 0.05$).

Table 3
Descriptive statistics of the relationship between simulated biomass from the LANDIS-II model and forest survey dataset (FSD) derived biomass in the aggradation phase of different subregions (forestry bureau) and the entire Lesser Khingan Mountains area. k and R^2 represent the slope of regression line and correlations of linear regressions, respectively. P-values from a t-test indicate significant differences between the two biomass datasets at the 0.05 alpha level. *RMSE* and *ME* represent the root mean square error and Nash-Sutcliffe index of mean error in comparison between FSD derived biomass and simulated biomass in the aggradation phase, respectively.

Regions	P-values	R^2	k	RMSE (Mg ha^{-1})	ME
ZH	0.16	0.88	1.08	37.53	0.20
HX1	0.24	0.89	1.20	35.37	−0.05
WYL	0.21	0.85	1.23	37.21	−0.30
TWH	0.24	0.94	1.07	31.89	0.35
SGL1	0.13	0.94	1.43	42.02	−0.74
XQ	0.19	0.90	0.99	36.27	0.22
YH	0.36	0.93	1.04	25.49	0.60
WY	0.41	0.89	0.90	25.63	0.61
HX2	0.26	0.87	0.93	33.10	0.41
TB	0.06	0.91	2.17	53.27	−7.63
SGL2	0.86	0.84	0.53	18.68	0.71
HB	0.18	0.97	1.09	32.56	0.32
LL	0.22	0.76	0.71	37.90	0.01
SGL3	0.16	0.82	1.08	41.29	−0.02
FL	–	–	–	–	–
SL	0.16	0.86	0.86	38.98	0.37
MX	0.21	0.89	1.02	34.98	0.40
CL	0.16	0.79	0.98	40.21	−0.06
WMH	0.36	0.81	0.84	30.37	0.47
JST	0.31	0.79	0.92	31.69	0.30
TL	0.40	0.92	1.05	23.87	0.72
LKM	0.67	0.90	1.14	17.56	0.76

1996), which has been a popular approach for forest biomass estimation in China (Fang and Chen, 2001; Fang et al., 1998; Huang et al., 2007). For the initial landscape, dynamics of forest biomass over time for the entire *LKM* and most subregions presented an “S”-shaped curve (Figs. 4 and 5). This curve was consistent with some previous studies (Poorter et al., 2006, 2012), which pointed out that a logistic regression exists between a tree's diameter at breast height (DBH) and its age. This logistic relationship was also demonstrated at the stand scale by simulating forest biomass and forest age, which suggests that the forest biomass-age curve obtained using the space-for-time substitution method has certain rationality. The small difference of the mean forest biomass (4.6 Mg ha^{-1}) between FSD (Table 1) and LANDIS-II simulation (Fig. 4) indicated that the initial parameterization of LANDIS-II model was reliable. Moreover, time series changes of biomass with forest age was generated through the space-for-time substitution method, which shows great potential in validating long-term predictions of FLMs.

Great differences existed in the spatial patterns of forest biomass, which increased in the southern *LKM* and decreased in the northern *LKM* (Fig. 7). The reasons are complex and can be attributed to the following two aspects. First, the distribution of species composition varies among regions. Broadleaved forests and coniferous forests are the dominant forest types of the southern and northern parts of *LKM,* respectively. In climate warming scenarios, it is expected that the growth of broadleaved forests will be enhanced while coniferous forest growth would be inhibited (Bu et al., 2008a). When climate is maintained, broadleaved trees have a tendency to replace coniferous trees (Fraser et al., 2007). Second, forest age is highly variable among regions. Most of the forests in the southern *LKM* are young secondary forests, while old-growth forests account for a considerable proportion in the northern *LKM* (Chen, 2003; Xiao et al., 2002; Xu et al., 2008). Therefore, biomass accumulation increases at a fast rate in southern *LKM,* while forest biomass in the northern part of *LKM* during the simulation is closer to a steady state.

We compared forest biomass between FSD derived biomass and LANDIS-II simulated biomass in 2000. FSD derived biomass is regarded as the approximation of the real forest biomass. LANDIS-II overestimates the forest biomass in north part of *LKM* while underestimates the forest biomass in central and north part of *LKM* (Fig. 6c). The overestimation (<−80 Mg ha^{-1}) of forest biomass in the south is mainly attributed to the forest's vulnerability to human activities. The south part of *LKM* area is adjacent to urban land and cropland where human activities are very intense, and selective logging might be conducted and cause biomass loss in branches and leaves. These factors cannot be simulated in LANDIS-II model, which calculates forest biomass only through the composition of species physiological conditions and age cohorts' existence. The underestimation areas (>80 Mg ha^{-1}) are mainly distributed in the central and north part of *LKM*. These areas are interior forest land where forest age is relative higher but tree density is lower. This cause LANDIS-II to underestimate the real forest biomass in central and north part of *LKM*.

In this study, forest age for the *LKM* and all subregions were obtained by calculating the mean values of the whole forested pixels of relevant area and then used to construct forest biomass-age curves. Although the method that we used to calculate the forest age of each subregion ignored the variations, it is still an effective approach to estimate forest age at such large extents. Forest biomass can be generally obtained by using tree biomass and age stand estimates, however, this relationship varies among tree species (Deng et al., 2012; Worbes, 1999). For the initial landscape, we did not have all these relationships of all tree species. Therefore, we used another dataset (timber volume), which is uniformly obtained from the entire landscape, to calculate forest biomass at large extents. This approach controls the uncertainty of the calculation of forest biomass to some extent and makes the space-for-time method more appropriate in the validation of forest biomass predictions from LANDIS-II.

Table 4
Simulated and forest survey dataset (FSD) derived mean maximum biomass (MMB) in the post-aggradation phase of different subregions (forestry bureau) and the entire Lesser Khingan Mountains area. Mean maximum biomass represents the mean biomass value in the post-aggradation phase. *Difference* represent the difference value between simulated mean maximum biomass from the LANDIS-II model and FSD derived biomass in 2000. Forest age at the post-aggradation is the age at which the forest enters the post-aggradation phase.

Regions	*MMB* (Mg ha^{-1})		*Difference* (Mg ha^{-1})	Forest age at the post-aggradation phase (years)
	Prediction in LANDIS-II	Forest survey dataset		
ZH	247.33	184.54	62.79	130
HX1	246.62	154.71	91.91	90
WYL	248.71	163.12	85.59	100
TWH	243.78	182.26	61.52	110
SGL1	239.06	151.24	87.82	100
XQ	236.24	177.50	58.74	100
YH	237.97	180.77	57.20	110
WY	244.47	184.62	59.85	100
HX2	240.02	182.54	57.48	100
TB	237.53	114.04	123.49	90
SGL2	237.49	143.24	94.25	80
HB	234.76	181.10	53.66	120
LL	244.07	183.29	60.78	100
SGL3	242.71	181.61	61.10	120
FL	252.78	229.52	23.26	110
SL	224.36	195.93	28.43	120
MX	236.06	201.94	34.12	130
CL	233.52	181.08	52.44	100
WMH	233.08	184.89	48.19	90
JST	222.68	175.79	46.89	100
TL	235.80	195.89	39.91	140
LKM	237.97	184.52	53.45	120

4.2. Validation performance of predictions of LANDIS-II model

The *t*-test result showed that the field observed biomass around 2011 and LANDIS-II simulated biomass in 2010 belong to a same population (Fig. 8). This result might provide some evidence that biomass predictions are in line with the actual biomass storage at the initial stage of simulation. However, some errors still existed in the validation of the biomass predictions of LANDIS-II model at the site scale. The linear correlation only explained a proportion ($R^2 = 0.47$) of variance, and observed biomass of most sampling sites were higher than the predicted biomass for those positions (Fig. 8). This difference may be attributed to two main reasons. Firstly, FLMs such as LANDIS-II and LANDIS Pro are not built to predict forest dynamics at a specific location because stochastic components are contained in the models (Mladenoff and He, 1999a; Scheller et al., 2007). Secondly, predicted biomass of LANDIS-II model was output at 90-m resolution which may include forest gaps, while observed biomass that was obtained from 20 m × 50 m sized plots generally do not contain forest gaps. This phenomenon is extremely obvious in some forest plots in which biomass was larger than 200 Mg ha^{-1}. These plots are commonly located in old-growth forests and are more likely to contain larger forest gaps (Mladenoff et al., 1993; Runkle, 1981; Schnitzer et al., 2000).

A comparison of forest biomass-age curves with the biomass predictions from the LANDIS-II model showed excellent model performance during the aggradation phase for the entire *LKM* and most subregions (Figs. 4 and 5). According to *t*-test results, there is no statistically significant difference between biomass from FSD and predictions of LANDIS-II model for all regions in the aggradation phase, except for *Fenglin* (*FL*) (Table 3). The results also demonstrated significant linear correlations between the two biomass datasets of these regions, and most linear correlations indicated that predicted biomass in the aggradation phase for most subregions in the *LKM* are consistent with the real biomass. Most regions' R^2 values were larger than 0.8 and most *k* values were close to 1. Although *RMSE* and *ME* results between the two biomass datasets in aggradation phase for most subregions varied in relatively large ranges (Table 3), the optimal values of *RMSE* and *ME* both emerged when we conducted analysis for the entire *LKM*. This finding demonstrates that the performance of the validation of biomass predictions in LANDIS-II model using space-for-time substitution method is enhanced when spatial extent increases, and it further proves that the main function of FLMs is simulating forest dynamics at landscape scale (Holling, 1992; Prentice et al., 1993).

Great differences existed between mean biomass estimates from the FSD and predictions from the LANDIS-II model during the steady state phase for the *LKM* and each subregion (Table 4). The simulated *MMB* is obviously overestimated. The main possible reason is that the real forest landscape in the *LKM* experienced severe deforestation (Wei et al., 2014), mostly in mature and old-growth forests, which is not simulated in this study. From another perspective, the difference indicates that the potential for biomass accumulation maybe increased by a considerable level if forest harvesting is forbidden. This finding may be an important reference for forest managers.

Further, we cannot neglect the simulation error of the model itself. The simulation of forest biomass by LANDIS-II may overestimate the biomass of the regions that already have high level of biomass in the initial year (Fig. 6). LANDIS-II model simulates forest biomass based on species cohorts amount and stand ages, which do not contain all possible factors that might be influencing forest biomass accumulation. Therefore, these factors may also cause the deviation between simulated biomass and FSD derived biomass. Moreover, uncertainties exist in the application of the space-for-time substitution method, which may also contribute to the difference between simulated biomass and FSD derived biomass in the post-aggradation phase. Temporal and spatial variation of climate, soil type, topography, forest management, and disturbances may exist in the study area. These factors all have impacts on the application of the space-for-time substitution method in predicting biodiversity, ecological succession, and soil development (Blois et al., 2013; Johnson and Miyanishi, 2008; Walker et al., 2010). In this study, although spatial heterogeneity of some forest growth conditions were reflected in the initial parameters of

LANDIS-II model, we cannot address all possible factors that might be influencing forest biomass accumulation in the simulation.

In the *LKM*, *Fenglin* (*FL*) is a natural reserve where the forests have been protected since the 1950s. Forest age composition of this subregion can sustainably remain constant, and the forest age as well as the biomass of most forests there remain at their maximum level (Table 1). This steady-state situation prohibits the detection of the aggradation in this subregion, and the space-for-time substitution method is not suitable for validation in this area. Moreover, forests in *FL* are commonly regarded as the climax stage of forest succession and used as a peak reference of carbon storage of forests of other places (Bu et al., 2008b; Zhou et al., 2007). This finding is demonstrated by the result of *MMB* in this study (Table 4), and it inspires us that the forest reserve is an area not only for biodiversity protection, but can also increase the carbon sink.

4.3. Implications of space-for-time substitution method

This study attempts to use the space-for-time substitution method to validate biomass predictions of a FLM at landscape scale. Forest biomass-age dynamic curves were used to compare long-term biomass predictions of the LANDIS-II model for the *LKM*, the results of which demonstrated an excellent applicability at the landscape scale. Nonetheless, before the age of 100 years, departure of the simulated biomass from biomass derived from FSD still exists in most subregions (Fig. 5). This divergence may be attributed to the following reason. The mean value of the forest stand age (Table 1) shows the general status of the forest age of a subregion. However, in order to match the time step of LANDIS-II (10 years) and to set each pair of biomass samples from FSD and LANDIS-II at the same time, the age of a subregion was set as integer times of 10 in the comparisons between the two biomass datasets. This may be a big problem and lead to departures in the final comparison between the two biomass datasets. If we horizontally move the start point of the biomass curve that was derived from FSD to the right position (mean forest stand age) as shown in Table 1, the departure may be reduced.

Our study is a new attempt to conduct validations of long-term predictions of FLMs at large spatial extents when only limited forest inventory data is available. Although data assimilation has been widely adopted to validate and calibrate the results of site-scale ecological models (Luo et al., 2014; Niu et al., 2014; Peng et al., 2011), it is still hard to apply data ingestion to evaluate predictions produced by landscape models due to a lack of long time series observation at the landscape scale. Moreover, forest inventory data in China is limited and commonly difficult to acquire. Thus, validating predictions of FLMs using the space-for-time substitution method is an appropriate approach in landscape ecology. It allows for the realistic comparison between observed results and long-term predicted results.

In order to simulate the real future state of forest landscape in *LKM*, no disturbance (forest harvest is banned in this area since 2000) was modeled in this study. However, historical disturbances like timber harvesting have a certain impact on current forests (Ghilardi et al., 2016; Law et al., 2004; Nepstad et al., 1999; Robichaud, 2000), and the effects of disturbances have been described by many previous studies at the landscape scale (Johnstone et al., 2010; Luo et al., 2014). In this study, we speculated that deforestation of old-growth forests had decreased the *MMB*, however, the mechanism and the degree of impacts from harvesting as well as other disturbances is still worth future study.

5. Conclusions

Biomass predictions from the LANDIS-II model from 2000 to 2300 was compared with FSD derived forest biomass at subregional and the landscape scales using the space-for-time substitution method in forest landscape of the *LKM*. Although it is impossible to exclude the spatial heterogeneity of the entire *LKM* landscape and among different subregions, the space-for-time substitution method is still been proved to have potential in validating time series biomass predictions of a FLM when only limited forest inventory data is available. Especially in the aggradation phase, high consistency exists between simulated biomass and FSD derived biomass. Moreover, predicted biomass at one time step is consistent with field observed biomass data at the site scale.

As to the heterogeneity of the biomass distribution of the initial landscape, forest reserve subregion (*FL*) stores more biomass than other areas of the *LKM*. The differences in species composition and forest age composition may cause great variation in biomass distribution during the simulation. Despite the simulation error of the model itself and the uncertainties in the application of space-for-time substitution method, considerable loss of biomass due to historical harvesting in *LKM* may be the most possible explanation of the difference between the mean maximum biomass of simulated biomass and FSD derived biomass.

Acknowledgements

This research was funded by Natural Science Foundation of China (41601181 and 41571408) and China Postdoctoral Science Foundation (2015M581519). We thank Yu Chang, Zaiping Xiong, and Miao Liu for their field work.

Appendix A. Supplementary data

Supplementary data related to this article can be found at http://dx.doi.org/10.1016/j.envsoft.2017.04.004.

References

Berec, L., Dolezal, P., Hais, M., 2013. Population dynamics of Ips typographus in the Bohemian Forest (Czech Republic): validation of the phenology model PHENIPS and impacts of climate change. For. Ecol. Manag. 292, 1–9.

Birdsey, R., Pregitzer, K., Lucier, A., 2006. Forest carbon management in the United States: 1600-2100. J. Environ. Qual. 35 (4), 1461–1469.

Blanco, J.A., Seely, B., Welham, C., Kimmins, J.P., Seebacher, T.M., 2007. Testing the performance of a forest ecosystem model (FORECAST) against 29 years of field data in a Pseudotsuga menziesii plantation. Can. J. For. Research-Revue Can. De Recherche For. 37 (10), 1808–1820.

Blois, J.L., Williams, J.W., Fitzpatrick, M.C., Jackson, S.T., Ferrier, S., 2013. Space can substitute for time in predicting climate-change effects on biodiversity. Proc. Natl. Acad. Sci. U. S. A. 110 (23), 9374–9379.

Bormann, F.H., Likens, G.E., 1979. Catastrophic disturbance and the steady-state in northern hardwood forests. Am. Sci. 67 (6), 660–669.

Bu, R., He, H.S., Hu, Y.M., Chang, Y., Larsen, D.R., 2008a. Using the LANDIS model to evaluate forest harvesting and planting strategies under possible warming climates in Northeastern China. For. Ecol. Manag. 254 (3), 407–419.

Bu, R.C., Chang, Y., Hu, Y.M., Li, X.Z., He, H.S., 2008b. Sensitivity of coniferous trees to environmental factors at different scales in the Small Xing'an Mountains, China. J. Plant Ecol. 32 (1), 80–87 (in Chinese).

Busing, R.T., Solomon, A.M., McKane, R.B., Burdick, C.A., 2007. Forest dynamics in Oregon landscapes: evaluation and application of an individual-based model. Ecol. Appl. 17 (7), 1967–1981.

Chave, J., 1999. Study of structural, successional and spatial patterns in tropical rain forests using TROLL, a spatially explicit forest model. Ecol. Model. 124 (2–3), 233–254.

Chen, C., Zhu, J., 1989. The Biomass Manual of Main Tree Species in Northeastern China. China Forestry Press, Beijing.

Chen, Y., 2003. Current state and development trend of vegetation in the Lesser Khingan Mountains area. North. Environ. 28 (2), 42–44 (in Chinese).

Chiang, J.-M., McEwan, R.W., Yaussy, D.A., Brown, K.J., 2008. The effects of prescribed fire and silvicultural thinning on the aboveground carbon stocks and net primary production of overstory trees in an oak-hickory ecosystem in southern Ohio. For. Ecol. Manag. 255 (5–6), 1584–1594.

Deng, H., Bu, R., Liu, X., He, W., Hu, Y., Huang, N., 2012. Simulating the effects of forestry classified management on forest biomass in Xiao Xing'an Mountains. Acta Ecol. Sin. 32 (21), 6679–6687 (in Chinese).

Dixon, R.K., Brown, S., Houghton, R.A., Solomon, A.M., Trexler, M.C., Wisniewski, J.,

1994. Carbon pools and flux of global forest ecosystems. Science 263 (5144), 185–190.
Dong, B., Feng, Z., Zhang, D., Yao, S., Sui, H., Wang, J., 2008. Construction Technology of Digital and Three-dimensional Forest Form Map Based on GIS. J. Beijing For. Univ. vol. 30 (1), 143–146 (in Chinese).
Fang, J.Y., Chen, A.P., 2001. Dynamic forest biomass carbon pools in China and their significance. Acta Bot. Sin. 43 (9), 967–973.
Fang, J.Y., Liu, G.H., Xu, S.L., 1996. Biomass and net production of forest vegetation in China. Acta Ecol. Sin. 16 (5), 497–508 (in Chinese).
Fang, J.Y., Wang, G.G., Liu, G.H., Xu, S.L., 1998. Forest biomass of China: an estimate based on the biomass-volume relationship. Ecol. Appl. 8 (4), 1084–1091.
Forestry Canada Fire Danger Group, 1992. In: Directorate, F.C.S.a.S.D. (Ed.), Development and Structure of the Canadian Forest Fire Behavior Prediction System. Information Report ST-x-3 (Ottawa, Ontario, Canada).
Fraser, S.E.M., Dytham, C., Mayhew, P.J., 2007. Determinants of parasitoid abundance and diversity in woodland habitats. J. Appl. Ecol. 44 (2), 352–361.
Gardner, R.H., Urban, D.L., 2003. Model validation and testing: past lessons, present concerns, future prospects.
Ghilardi, A., Bailis, R., Mas, J.-F., Skutsch, M., Alexander Elvir, J., Quevedo, A., Masera, O., Dwivedi, P., Drigo, R., Vega, E., 2016. Spatiotemporal modeling of fuelwood environmental impacts: towards improved accounting for non-renewable biomass. Environ. Model. Softw. 82, 241–254.
Gustafson, E.J., Shifley, S.R., Mladenoff, D.J., Nimerfro, K.K., He, H.S., 2000. Spatial simulation of forest succession and timber harvesting using LANDIS. Can. J. For. Research-Revue Can. De Recherche For. 30 (1), 32–43.
Gustafson, E.J., Shvidenko, A.Z., Sturtevant, B.R., Scheller, R.M., 2010. Predicting global change effects on forest biomass and composition in south-central Siberia. Ecol. Appl. 20 (3), 700–715.
He, H.S., 2008. Forest landscape models: definitions, characterization, and classification. For. Ecol. Manag. 254 (3), 484–498.
He, H.S., Hao, Z.Q., Mladenoff, D.J., Shao, G.F., Hu, Y.M., Chang, Y., 2005. Simulating forest ecosystem response to climate warming incorporating spatial effects in north-eastern China. J. Biogeogr. 32 (12), 2043–2056.
He, H.S., Mladenoff, D.J., 1999. Spatially explicit and stochastic simulation of forest-landscape fire disturbance and succession. Ecology 80 (1), 81–99.
He, H.S., Mladenoff, D.J., Crow, T.R., 1999. Linking an ecosystem model and a landscape model to study forest species response to climate warming. Ecol. Model. 114 (2–3), 213–233.
Holling, C.S., 1992. Cross-scale morphology, geometry, and dynamics of ecosystems. Ecol. Monogr. 62 (4), 447–502.
Houghton, R.A., Hackler, J.L., 2000. Changes in terrestrial carbon storage in the United States. 1: the roles of agriculture and forestry. Glob. Ecol. Biogeogr. 9 (2), 125–144.
Huang, C.-D., Yang, W.-Q., Tang, X., 2007. Spatiotemporal variation of carbon storage in forest vegetation in Sichuan Province. Chin. J. Appl. Ecol. 18 (12), 2687–2692.
Johnson, E.A., Miyanishi, K., 2008. Testing the assumptions of chronosequences in succession. Ecol. Lett. 11 (5), 419–431.
Johnstone, J.F., Hollingsworth, T.N., Chapin III, F.S., Mack, M.C., 2010. Changes in fire regime break the legacy lock on successional trajectories in Alaskan boreal forest. Glob. Change Biol. 16 (4), 1281–1295.
Keith, H., Mackey, B.G., Lindenmayer, D.B., 2009. Re-evaluation of forest biomass carbon stocks and lessons from the world's most carbon-dense forests. Proc. Natl. Acad. Sci. U. S. A. 106 (28), 11635–11640.
Larsen, D.R., Dey, D.C., Faust, T., 2010. A stocking diagram for midwestern eastern cottonwood-silver maple-american sycamore bottomland forests. North. J. Appl. For. 27 (4), 132–139.
Law, B.E., Turner, D., Campbell, J., Sun, O.J., Van Tuyl, S., Ritts, W.D., Cohen, W.B., 2004. Disturbance and climate effects on carbon stocks and fluxes across Western Oregon USA. Glob. Change Biol. 10 (9), 1429–1444.
Li, C., Flannigan, M.D., Corns, I.G.W., 2000. Influence of potential climate change on forest landscape dynamics of west-central Alberta. Can. J. For. Research-Revue Can. De Recherche For. 30 (12), 1905–1912.
Luo, X., He, H.S., Liang, Y., Wang, W.J., Wu, Z., Fraser, J.S., 2014. Spatial simulation of the effect of fire and harvest on aboveground tree biomass in boreal forests of Northeast China. Landsc. Ecol. 29 (7), 1187–1200.
Ma, J., Bu, R.C., Deng, H.W., Hu, Y.M., Qin, Q., Han, F.L., 2014a. Simulating climate change effect on aboveground carbon sequestration rates of main broad-leaved trees in the Small Khingan Mountains area, Northeast China. Chin. J. Appl. Ecol. 25 (9), 1106–1116 (in Chinese).
Ma, J., Bu, R.C., Liu, M., Chang, Y., Qin, Q., Hu, Y.M., 2015. Ecosystem carbon storage distribution between plant and soil in different forest types in Northeastern China. Ecol. Eng. 81, 353–362.
Ma, J., Hu, Y., Bu, R., Chang, Y., Deng, H., Qin, Q., 2014b. Predicting impacts of climate change on the aboveground carbon sequestration rate of a temperate forest in northeastern China. Plos One 9 (4).
Marcot, B.G., Steventon, J.D., Sutherland, G.D., McCann, R.K., 2006. Guidelines for developing and updating Bayesian belief networks applied to ecological modeling and conservation. Can. J. For. Research-Revue Can. De Recherche For. 36 (12), 3063–3074.
McMahon, S.M., Parker, G.G., Miller, D.R., 2010. Evidence for a recent increase in forest growth. Proc. Natl. Acad. Sci. U. S. A. 107 (8), 3611–3615.
Miehle, P., Livesley, S.J., Li, C.S., Feikema, P.M., Adams, M.A., Arndt, S.K., 2006. Quantifying uncertainty from large-scale model predictions of forest carbon dynamics. Glob. Change Biol. 12 (8), 1421–1434.
Mladenoff, D.J., 2004. LANDIS and forest landscape models. Ecol. Model. 180 (1), 7–19.
Mladenoff, D.J., He, H.S., 1999a. Design and Behavior of LANDIS, an Objectoriented Model of Forest Landscape Disturbance and Succession. Cambridge University Press, Cambridge, UK.
Mladenoff, D.J., He, H.S., 1999b. Design, Behavior and Application of LANDIS, an Object Oriented Model of Forest Landscape Disturbance and Succession Cambridge University Press, Cambridge.
Mladenoff, D.J., White, M.A., Pastor, J., Crow, T.R., 1993. Comparing spatial pattern in unaltered old-growth and disturbed forest landscapes. Ecol. Appl. 3 (2), 294–306.
Nepstad, D.C., Verissimo, A., Alencar, A., Nobre, C., Lima, E., Lefebvre, P., Schlesinger, P., Potter, C., Moutinho, P., Mendoza, E., Cochrane, M., Brooks, V., 1999. Large-scale impoverishment of Amazonian forests by logging and fire. Nature 398 (6727), 505–508.
Niu, S.L., Luo, Y.Q., Dietze, M.C., Keenan, T.F., Shi, Z., Li, J.W., Chapin, F.S., 2014. The role of data assimilation in predictive ecology. Ecosphere 5 (5).
Peng, C., Guiot, J., Wu, H., Jiang, H., Luo, Y., 2011. Integrating models with data in ecology and palaeoecology: advances towards a model-data fusion approach. Ecol. Lett. 14 (5), 522–536.
Perry, D.A., Oren, R., Hart, S.C., 2008. Forest ecosystems. Johns Hopkins University Press.
Poorter, H., Niklas, K.J., Reich, P.B., Oleksyn, J., Poot, P., Mommer, L., 2012. Biomass allocation to leaves, stems and roots: meta-analyses of interspecific variation and environmental control. New Phytol. 193 (1), 30–50.
Poorter, L., Bongers, L., Bongers, F., 2006. Architecture of 54 moist-forest tree species: traits, trade-offs, and functional groups. Ecology 87 (5), 1289–1301.
Prentice, I.C., Sykes, M.T., Cramer, W., 1993. A simulation-model for the transient effects of climate change on forest landscapes. Ecol. Model. 65 (1–2), 51–70.
R Development Core Team, 2011. R: a language and environment for statistical computing. R foundation for statistical computing, Vienna p.
Robichaud, P.R., 2000. Fire effects on infiltration rates after prescribed fire in Northern Rocky Mountain forests, USA. J. Hydrology 231, 220–229.
Runkle, J.R., 1981. Gap regeneration in some old-growth forests of the eastern-united-states. Ecol. 62 (4), 1041–1051.
Saatchi, S.S., Harris, N.L., Brown, S., Lefsky, M., Mitchard, E.T.A., Salas, W., Zutta, B.R., Buermann, W., Lewis, S.L., Hagen, S., Petrova, S., White, L., Silman, M., Morel, A., 2011. Benchmark map of forest carbon stocks in tropical regions across three continents. Proc. Natl. Acad. Sci. U. S. A. 108 (24), 9899–9904.
Scheller, R.M., Domingo, J.B., Sturtevant, B.R., Williams, J.S., Rudy, A., Gustafson, E.J., Mladenoff, D.J., 2007. Design, development, and application of LANDIS-II, a spatial landscape simulation model with flexible temporal and spatial resolution. Ecol. Model. 201 (3–4), 409–419.
Scheller, R.M., Hua, D., Bolstad, P.V., Birdsey, R.A., Mladenoff, D.J., 2011a. The effects of forest harvest intensity in combination with wind disturbance on carbon dynamics in Lake States Mesic Forests. Ecol. Model. 222 (1), 144–153.
Scheller, R.M., Mladenoff, D.J., 2004. A forest growth and biomass module for a landscape simulation model, LANDIS: design, validation, and application. Ecol. Model. 180 (1), 211–229.
Scheller, R.M., Van Tuyl, S., Clark, K., Hayden, N.G., Hom, J., Mladenoff, D.J., 2008. Simulation of forest change in the New Jersey Pine Barrens under current and pre-colonial conditions. For. Ecol. Manag. 255 (5–6), 1489–1500.
Scheller, R.M., Van Tuyl, S., Clark, K.L., Hom, J., La Puma, I., 2011b. Carbon sequestration in the New Jersey pine barrens under different scenarios of fire management. Ecosyst. 14 (6), 987–1004.
Schmitz, O.J., 1997. Press perturbations and the predictability of ecological interactions in a food web. Ecol. 78 (1), 55–69.
Schnitzer, S.A., Dalling, J.W., Carson, W.P., 2000. The impact of lianas on tree regeneration in tropical forest canopy gaps: evidence for an alternative pathway of gap-phase regeneration. J. Ecol. 88 (4), 655–666.
Shifley, S.R., Rittenhouse, C.D., Millspaugh, J.J., Millspaugh, J.J., Thompson, F.R., 2009. Validation of landscape-scale decision support models that predict vegetation and wildlife dynamics.
Tian, S., Youssef, M.A., Chescheir, G.M., Skaggs, R.W., Cacho, J., Nettles, J., 2016. Development and preliminary evaluation of an integrated field scale model for perennial bioenergy grass ecosystems in lowland areas. Environ. Model. Softw. 84, 226–239.
Tsoar, A., Allouche, O., Steinitz, O., Rotem, D., Kadmon, R., 2007. A comparative evaluation of presence-only methods for modelling species distribution. Divers. Distrib. 13 (4), 397–405.
Walker, L.R., Wardle, D.A., Bardgett, R.D., Clarkson, B.D., 2010. The use of chronosequences in studies of ecological succession and soil development. J. Ecol. 98 (4), 725–736.
Wang, C.K., 2006. Biomass allometric equations for 10 co-occurring tree species in Chinese temperate forests. For. Ecol. Manag. 222 (1–3), 9–16.
Wang, F.G., Mladenoff, D.J., Forrester, J.A., Blanco, J.A., Scheller, R.M., Peckham, S.D., Keough, C., Lucash, M.S., Gower, S.T., 2014a. Multimodel simulations of forest harvesting effects on long-term productivity and CN cycling in aspen forests. Ecol. Appl. 24 (6), 1374–1389.
Wang, W.J., He, H.S., Spetich, M.A., Shifley, S.R., Thompson III, F.R., Dijak, W.D., Wang, Q., 2014b. A framework for evaluating forest landscape model predictions using empirical data and knowledge. Environ. Model. Softw. 62, 230–239.
Wei, Y.W., Zhou, W.M., Yu, D.P., Zhou, L., Fang, X.M., Zhao, W., Bao, Y., Meng, Y.Y., Dai, L.M., 2014. Carbon storage of forest vegetation under the natural forest protection program in northeast China. Acta Ecol. Sin. 34 (20), 5696–5705.

Worbes, M., 1999. Annual growth rings, rainfall-dependent growth and long-term growth patterns of tropical trees from the Caparo Forest Reserve in Venezuela. J. Ecol. 87 (3), 391–403.

Xiao, X.M., Boles, S., Liu, J.Y., Zhuang, D.F., Liu, M.L., 2002. Characterization of forest types in Northeastern China, using multi-temporal SPOT-4 VEGETATION sensor data. Remote Sens. Environ. 82 (2–3), 335–348.

Xu, C.-Y., Turnbull, M.H., Tissue, D.T., Lewis, J.D., Carson, R., Schuster, W.S.F., Whitehead, D., Walcroft, A.S., Li, J., Griffin, K.L., 2012. Age-related decline of stand biomass accumulation is primarily due to mortality and not to reduction in NPP associated with individual tree physiology, tree growth or stand structure in a Quercus-dominated forest. J. Ecol. 100 (2), 428–440.

Xu, C.G., Gertner, G.Z., Scheller, R.M., 2007. Potential effects of interaction between CO2 and temperature on forest landscape response to global warming. Glob. Change Biol. 13 (7), 1469–1483.

Xu, W.D., He, X.Y., Chen, W., Liu, C.F., Zhao, G.L., Zhou, Y., 2008. Ecological division of vegetation in Northeastern China. Chin. J. Ecol. 27 (11), 1853–1860 (in Chinese).

Zaniewski, A.E., Lehmann, A., Overton, J.M.C., 2002. Predicting species spatial distributions using presence-only data: a case study of native New Zealand ferns. Ecol. Model. 157 (2–3), 261–280.

Zhang, G., Wang, Q., Zhang, F., Wu, K., Cai, C., Zhang, M., Li, D., Zhao, Y., Yang, J., 2013. Criteria for establishment of soil family and soil series in Chinese soil taxonomy. Acta Pedol. Sin. 50 (4), 826–834.

Zhou, D.H., He, H.S., Li, X.Z., Zhou, C.H., Wang, X.G., Chen, H.W., 2007. Potential response of different stand age classes to climate change in the Xiao Xing'an Mountains, northeastern China. J. Beijing For. Univ. 29 (4), 110–117 (in Chinese).